Thermal-Electrochemical Modeling and Analysis of Different Cathode-Anode Pairs for Lithium-ion Battery

Snigdha SHARMA[1], Amrish K. PANWAR[2], Madan Mohan TRIPATHI[1]
[1]*Department of Electrical Engineering, Delhi Technological University, New Delhi, India*
[2]*Department of Applied Physics, Delhi Technological University, New Delhi, India*
mmtripathi@dce.ac.in

***Abstract*—This article represents a computational approach for the estimation of the characteristics of lithium-ion batteries for a 2D electrochemical model of cylindrical type lithium-ion battery using COMSOL software. Various input parameters used in the model formulation have been obtained from experimental data as well as published work. For the evaluation of battery performance, an electrochemical-thermal mathematical model has been designed to determine the electrochemical parameters such as rate capability, charge/ discharge characteristic, ragone curve. Further, the electrochemical characteristics have been characterized with the help of cyclic voltammetry (CV) test which indicates the uniform electrochemical reactivity and transport properties of the designed battery. Two types of electrode pairs in which $LiMn_2O_4$ as cathode materials form $LiMn_2O_4$ (LMO)/Graphite and LMO/Carbon (MCMB) are designed and these electrode pairs are simulated and evaluated to determine the characteristics of battery material using charge and discharge curve at different current loads (C-rates) as well as ragone curve. The simulation results validate the electrochemical behavior of the proposed 2D model. Also, the LMO/graphite electrode pair shows better discharging and charging capacity, high energy, and power curve as compared to the LMO/Carbon (MCMB) electrode pair.**

***Index Terms*—anode, batteries, cathode, electrochemical, electrodes.**

I. INTRODUCTION

Nowadays, Electrochemical Energy Storage (EES) devices are becoming important due to their good life cycle, high energy density, reliability, stability, etc. [1-5].

Rechargeable batteries are the most useful and popular EES device as it gives the best comprehensive performance in the commercialized segments such as portable electronic devices, electric vehicles for transportation, communications and many more [5-7].

Among different types of rechargeable batteries, Lithium-ion batteries (LIBs) give the best comprehensive performance but, due to the physical limitation of the electrode material still, the application of these batteries is limited [7-8]. The ionic and electronic conduction, as well as transport phenomenon of the LIBs, are the major focus area of research as the ionic and electronic conduction of LIBs are strongly related to the rate capability of the battery [9].

This work was supported by LIBT Lab, Department of Applied Physics, Delhi Technological University, New Delhi to carry out this research work.

A. Li-ion Transport Mechanism

In LIBs, both cathode and anode electrode materials together reveal the ionic and electronic conduction properties of the battery [10]. It is very difficult to improve the ionic conduction of the material because it is strongly related to the ionic transport species that directly represents the composition and structure of the material [11-12]. To improve these properties, certain technical methods are used which help to enhance the intrinsic electronic conductivity of the material through adding a conduction additive or carbon coating, etc. [13]. There are various factors related to ionic transport such as electric field gradient, concentration gradient, and chemical potential gradient [14]. The ionic transport mechanism is generally associated with macroscopic diffusion or related to the movement of Li ions when the external electric potential was applied to the battery. This diffusion coefficient relationship can be explained with the help of the Nernst-Einstein equation 1.

$$\frac{\sigma_i}{D_i} = \frac{F^2 C_i Z_i^2}{RT} \tag{1}$$

where σ_i is the ionic conductivity of species i, D_i is the chemical diffusion coefficient of species i, Z_i is the charge of species i, F is faraday's constant, T is the absolute temperature, R is the gas constant [1].

Further, the mobility of ions u_i is linked to the diffusion coefficient of ions D_i as shown in equation 2.

$$D_i = Tu_i k_b \tag{2}$$

where k_b is the Boltzmann's constant and T is the temperature in Kelvin [10].

The diffusion in solids takes place through the movement of ions when an adjacent site of the atom is empty or displacement of atoms causing lattice distortion and have sufficient energy to break bonds with its neighbor atoms [10-15]. But in the case of material used in LIB, the diffusion mechanism is more complex which is analyzed by various factors such as the motion of atoms, thermal energy, vacancy at the adjacent site, sufficient energy to break the bond, and many more [10], [15-16]. Therefore, the electronic conduction mechanism of LIBs becomes the focus area of concern.

B. Electronic Conduction Mechanism

Electron transport in the solid electrode is one of the most important factors in the evaluation of the rate performance of the battery [12] [14]. In LIBs, when the charging and

Digital Object Identifier 10.4316/AECE.2021.03007

discharging process takes place, electrons must be transferred from the cathode to anode material via an external circuit and it also helps to describe the electrical conductivity of the electrode material [15][16]. The electrical conduction is represented as a flow of free electrons when an external field is applied under the equilibrium state. The electrical conductivity can be obtained from the given equation 3.

$$\sigma = \frac{N_f e^2 \tau}{m} \tag{3}$$

where N_f is a number of free electrons, e is the charge of electrons, σ is the electrical conductivity, m is the mass of electrons, and τ is relaxation time [10].

The classic electron transport theory and quantum transport theory are two approaches that have been developed to describe the electron conduction characteristics of LIBs [10]. According to band theory, the electronic structure of anode material in LIBs has a large number of free electrons and the Fermi level also lies within the conduction band [10-11]. The transport of electrons in anode material is fast and its conductivity also lies in the range of 10^4 $s.cm^{-1}$ whereas in the case of cathode material, its electronic structure lies in the range of insulating material and its conduction is low under normal temperature [5], [16]. Thermal excitation is required to generate conduction across charge carriers due to which its conductivity also increases. Hence, the doping technique has been used widely to enhance the electrical conductivity of the material.

For electrode material, the free-electron mechanism also depends upon the small polaron conduction, which was proposed to describe the concept of electron-phonon interaction on dielectric crystals [10]. It reduces the electron mobility because of the localization effect or trapping the electron on the polaron state. For example, in $LiMn_2O_4$ cathode material, Mn atoms are shared with an average oxidation state of $Mn^{3.5+}$. However, in this case, the localize (trap) effect on electrons has been considered on the 3d orbital of Mn atoms in which oxidation takes place and exhibits half of Mn^{3+} atom on one part and another half Mn^{4+} atom [10-16]. In Mn-3d-z^2 orbital excess electrons were hold than Mn^{4+}, which lower the energy of the crystal due to local lattice Jahn-Teller distortion [10], [12]. Hence, the polaron state transport charge and localizes the electron due to the lattice distortion which leads to lower the mobility of electrons [10-11].

In LIBs, the polaron conduction phenomenon helps to understand the electrical conductivity of compounds but it was very difficult to analyze the polaron state experimentally and only the computation tools such as DFT+U have been used to study this problem [10]. The formation of battery models also helps in getting a better understanding of battery's performances such as safety, efficiency, and stability [11-12]. Electrochemical-thermal models are preferred to optimize battery performance during the charging and discharging process.

A lot of work has been done by various researchers on battery modeling. A 1-D theoretical battery model has been developed to investigate particle size distribution on the porous intercalation electrodes [11-13]. A Pseudo-two-dimensional (P2D) model for cylindrical Li-ion Battery has also been developed using the FORTRAN code [11-15] and the electronic and ionic conductivity of the material were enhanced [16-17]. Newman et al. and his co-workers developed many models for Li-ion batteries to analyze the porosity and thickness of electrodes [18]. The capacity improvement was carried out by a gradient-based optimization model [17-19]. Also, the study of parameter sensitivity helps us to know the performance of the battery based on its design factors and variables for specific power and energy [20].

In this study, the electrochemical model for LIB has been designed on COMSOL Multiphysics software. An electrode pair has been developed which looks like a sandwich model of five different layers. The proposed layered structure has been used to validate the mathematical model of a $LiMn_2O_4$ /MCMB and $LiMn_2O_4$/graphite cylindrical battery for various parameters. The validated model was designed in such a way, that this can be implemented for the experimental process of a cell. Statistical analysis has been done to optimize the cell performance with the help of various parameters such as electrode thickness (L_{pos}), particle size (r_p), active material volume fraction, and C-rates. This analysis demonstrates the $LiMn_2O_4$ cathode material characteristics, with two different types of anode material one at a time. Hence, a comparative study on $LiMn_2O_4$ has been carried out to understand the battery characteristics using COMSOL Multi-physics.

II. Two-Dimensional Pseudo Model Formulation

The P2D electrochemical thermal model of a Lithium-ion battery has been implemented with the help of the electrochemical domain [12]. This model is based on a few fundamentals of batteries such as the transport mechanism, electrochemical kinetics, and thermodynamics, which helps to evaluate rate capability as well as characteristics of the battery [1], [12].

A 2D Li-ion battery architecture has been designed for simulation. In this design, a cylindrical battery has been made up of a number of cylindrical cells where every cylindrical cell has to be connected in parallel by the positive and negative terminal of the battery. Every cell was designed like a sandwich model of five different layers which was sequentially followed by a positive current collector (Aluminum), a positive electrode ($LiMn_2O_4$), separator (microporous polypropylene celgard 2400), a negative electrode (Graphite/Carbon), and negative current collector (Copper) as shown in Fig. 1. This theoretical model was based on an experimentally validated model [11]. In this model two types of anode materials, graphite and carbon (MCMB) were used to obtain a cathode material characteristic. The model was formulated to evaluate the $LiMn_2O_4$ cathode material performance during the charging and discharging process.

For model formulation, various input parameters such as geometry design parameters for model layout, both anode and cathode material properties, ambient operating temperature with different boundary conditions and load current have been considered. These input parameters are listed in Table I.

TABLE I. MEASURED AND MODEL INPUT PARAMETERS FOR THE BATTERY [16, 17, 18, 20, 21]

Name	Units/Equation	Description
Rp_neg	2.50e-6[m]	Particle radius negative electrode
Rp_pos	1.70e-6[m]	Particle radius positive electrode
Epss_pos 1-Epsl_pos	-0.170	Solid phase volume fraction positive electrode
Epsl_pos	0.400	Electrolyte phase volume fraction positive electrode
Brugl_pos	2.98	Bruggeman coefficient for tortuosity in the positive electrode
Epss_neg 1-Epsl_neg	-0.172	Solid phase volume fraction negative electrode
Epsl_neg	0.444	Electrolyte phase volume fraction negative electrode
Epsl_sep	0.370	Electrolyte phase volume fraction separator
Brugl_sep	3.15	Bruggeman coefficient for tortuosity in separator
K_neg	2e-11[m/s]	Reaction rate coefficient negative electrode
K_pos	5e-10[m/s]	Reaction rate coefficient positive electrode
Cs0_neg	2205	Initial state-of-charge negative electrode
Cs0_pos	20925	Initial state-of-charge positive electrode
Cl_0	1200[mol/m^3]	Initial electrolyte salt concentration
a	7.5	C-factor
I_1C	12[A/m^2]	1C discharge current
I_load	i_1C*a	Charge/discharge current
L_neg	55e-6[m]	Length of negative electrode
L_sep	70e-6[m]	Length of separator
L_pos	55e-6[m]	Length of positive electrode
D_can	0.25[mm]	The thickness of the battery canister
R_batt	9[mm]	Battery radius
H_batt	65[mm]	Battery height
R_mandrel	2[mm]	Mandrel radius
L_neg_cc	7[um]	Negative current collector thickness
L_pos_cc	10[um]	Positive current collector thickness
L_batt	L_neg+L_neg_cc +L_sep+L_pos+L_pos_cc	Cell thickness
K_T_pos	1.58[W/(m*K)]	Positive electrode thermal conductivity
K_T_neg	1.04[W/(m*K)]	Negative electrode thermal conductivity
K_T_pos_cc	170[W/(m*K)]	Positive current collector thermal conductivity
K_T_neg_cc	398[W/(m*K)]	Negative current collector thermal conductivity
K_T_sep	0.344[W/(m*K)]	Separator thermal conductivity
Rho_pos	2328.5[kg/m^3]	Positive electrode density
Rho_neg	1347.33[kg/m^3]	Negative electrode density
Rho_pos_cc	2770[kg/m^3]	Positive current collector density
Rho_neg_cc	8933[kg/m^3]	Negative current collector density
Rho_sep	1008.98[kg/m^3]	Separator density
Cp_pos	1269.21[J/(kg*K)]	Positive electrode heat capacity
Cp_neg	1437.4[J/(kg*K)]	Negative electrode heat capacity
Cp_pos_cc	875[J/(kg*K)]	Positive current collector heat capacity
Cp_neg_cc	385[J/(kg*K)]	Negative current collector heat capacity
Cp_sep	1978.16[J/(kg*K)]	Separator heat capacity
K_T_batt_ang	(K_T_pos*L_pos+ K_T_neg*L_neg+ K_T _pos_cc*L_pos_cc+ K_T_neg_cc*L_neg_cc+ K_T_sep*L_sep)/L_batt	Battery thermal conductivity, angular
K_T_batt_r	L_batt/(L_pos/ K_T _pos+L_neg/ K_T _neg+L_pos_cc/ K_T _pos_cc+L_neg_cc/ K_T_neg_cc+L_sep / K_T_sep)	Battery thermal conductivity, radial
Rho_batt	(rho_pos*L_pos+ rho_neg*L_neg+rho_pos_cc*L_pos_cc+rho_neg_cc* L_neg_cc+rho_sep*L_sep)/L_batt	Battery density
Cp_batt	(Cp_pos*L_pos+ Cp_neg*L_neg+Cp_pos_cc*L_pos_cc+Cp_neg_cc*L_neg_cc+Cp_sep* L_sep)/L_batt	Battery heat capacity
Cycle_time	600[s]	Cycle time
T_inlet ""	298.15[K]	Inlet temperature
T_init	T_inlet	Initial temperature
H_connector	3[mm]	connector height
R_connector	3[mm]	connector radius
S_inlet	2*R_batt	Length of inlet flow region
S_matrix	3*R_batt	Battery-battery distance in matrix
V_in	0.1[m/s]	Inlet velocity
t	0	Time parameter in the initialization study step

Some other influential input parameters such as the stoichiometry of the model for both positive and negative electrodes, electrodes charge transfer coefficient, electrolyte coefficient, Bruggeman coefficient are taken from the data available in the literature [16-20]. In this proposed theoretical model, the Li-ions transport phenomenon is based on parameters such as solid-state potential, electrolyte concentration, solid-state concentration within the electrode, and electrolyte potential within the separator. These domains are further explained with the help of mathematical modeling presented in the following section.

III. ELECTROCHEMICAL-THERMAL MATHEMATICAL MODELING

The proposed electrochemical-thermal model has some governing equations and boundary conditions which help to

evaluate the certain variables for solving the pseudo-two-dimensional model such as electrochemical kinetics, electric charge conservation, energy conservation, and mass conservation [21-24]. For the simulation of solid-state lithium-ion battery and analyzing its chemistry domain, certain electrochemical kinetics equations were carried out with the help of the Butler-Volmer governing equation [25-26], which is used to describe the lithium concentration as well as charge distribution on the anode and cathode electrodes and electrolyte phase as shown in equation 4.

$$j^{li} = a_s i_o \left[\exp\left(\frac{\alpha_a F}{RT}\eta\right) - \exp\left(\frac{-\alpha_c F}{RT}\eta\right)\right] \quad (4)$$

where j^{li} refers to a reaction current density, a_s is the reaction surface area [23-25].

Further, the electrodes having a solid active phase and electrolyte as a liquid phase which together creates an interfacial area and known as reaction surface area (a_s) are shown with equation 5.

$$a_s = \frac{3\varepsilon_s}{r_p} = \left(\frac{1-\varepsilon_e-\varepsilon_f}{r_p}\right) \quad (5)$$

where N_p represents the number of spheres per unit volume, ε_s is the active material volume fraction, ε_e is the electrode porosity, r_p is the radius of the active material and ε_f is the fillers of the active material [26].

The relation of the lithium concentration for the potential of both the electrodes is defined with the help of current density (i_o) and it is expressed as equation 6.

$$i_o = k_i (c_e)^{\alpha_a} \left(C_{surf,\max} - C_{surf,e}\right)^{\alpha_a} \left(C_{surf,e}\right)^{\alpha_c} \quad (6)$$

where k_i denoted the temperature-dependent reaction rate, α_a, α_c is the symmetry factor, C_e, C_s are lithium concentration in the solid and electrolyte phase and $C_{surf,\,max}$, $C_{surf,\,e}$ is the lithium concentration maximum on the surface and electrolyte [26-27].

The electronic charge balance has to be maintained with the equivalence of Li-ions during lithiation and de-lithiation and electron flow in the charging and discharging process. The amount of potential in the solid phase has to be a function of electrode conductivity and reaction current density as shown in the equation 7.

$$\tilde{N}\left(\sigma^{eff}\tilde{N}\varphi_s\right) = j^{li} \quad (7)$$

where φ_s is the potential in the solid phase [27-28].

Similarly, the potential in the liquid electrolyte is dependent on the concentration of the lithium ions and the current density, which is explained with the help of the equation 8.

$$\tilde{N}\left(\sigma^{eff}\tilde{N}\varphi_e\right) + \tilde{N}\left(k_d^{eff}\tilde{N}\ln(c_e)\right) + j^{li} = 0 \quad (8)$$

where σ^{eff} is the effective conductivity and $k_D{}^{eff}$ represents the effective diffusional conductivity of the species, and φ_e is the potential in the electrolyte phase [26-28].

For maintaining the mass conservation in the solid phase, it was assumed that the particle size of the electrode material in the model has to be identical and lithium-ion distribution has to be explained with the help of Fick's law of concentration gradient as given in equation 9.

$$\frac{\P c_s}{\P x} = \frac{D_s}{r^2}\frac{\P\left(r^2\frac{\P c_s}{\P r}\right)}{\P r} \quad (9)$$

where D_s is the diffusion coefficient in the solid phase, r is the radius of the material [19] [20].

In this electrochemical simulation analysis, the domain equations help to implement the chemical transport equations for the reactant and product species [25]. This further demonstrates the electrochemical reactivity and the transport property of the battery [25-29]. However, this model was formulated with all the domain equations, which have been shown in the meshed structure of solid-state cylindrical type lithium-ion battery (LIB).

A. Model Meshed Structure

A 2D cylindrical Lithium-ion battery simulation model has been designed on a COMSOL Multi-physics 5.3a version to evaluate the battery performance in terms of rate capability. The model formulation parameters are explained in the above sections. In this model, various characteristics are demonstrated with the help of mathematical modeling. For example, the kinetics of mass transport in the LIBs, the lithium-ion diffusion is demonstrated with the help of Faraday's equation and the amount of energy and power in the battery is calculated using ragone plot [29]. The simulation results were generated with the help of the proposed 2D model and the experimental data were validated from the published literature [28-30].

Initially, the geometry of the model was designed considering different components such as porous electrodes, electrolytes, and current collectors. Then, the various governing equations were estimated for the 2D structure of the model for a better understanding of the ionic/ electronic conductivity phenomenon and mass transfer mechanism of the battery [31].

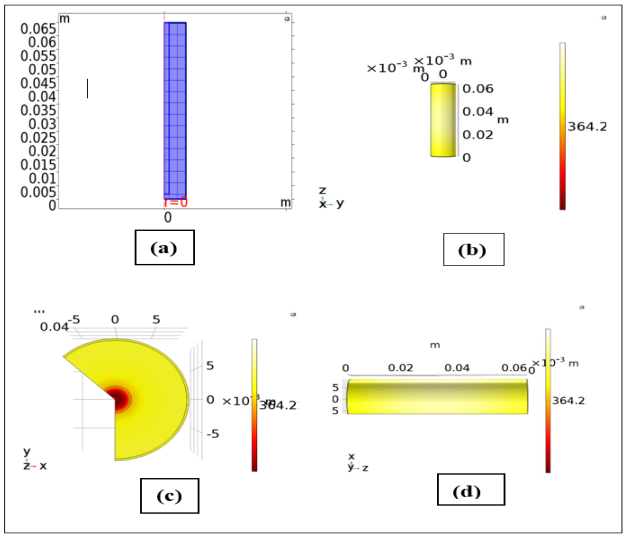

Figure 1. (a) Meshed geometry of cylindrical battery (b), (c), and (d) 2D cylindrical battery view along the YZ axis, XY axis, and ZX axis respectively

After including the all-necessary operational parameters, a meshed structure of the 2D model was obtained and this structure was analyzed in all three directions with ambient temperature and different boundary conditions [30-32]. This meshed structure is mapped with the help of a singular matrix as shown in Fig. 1 (a). Further, evaluation has been

carried out in the form of a 2D revolution model along with the combination of XY, YZ, ZX axis as shown in Fig. 1 (b), (c), (d) respectively.

This meshed structure indicates a blue dotted line which represents the triangular mapped domain on model geometry with the certain boundary condition at the corner of the battery. After setting up the mathematical geometry and meshing domain, the study has been performed with the help of parametric function. In this electrochemical-thermal model, cyclic voltammetry has been recorded on the electrode surface where potential is varying linearly as a function of time. Further, the comparative results on the rate capability of the battery are determined for various anode materials at different C-rates [31-35]. In this evaluation, the battery has been fully-charged and fully-discharged for investigating the ragone plot to calculate the energy and power outputs from the battery. The results were simulated on 2D and 1D geometry plot groups, which is illustrated in the next section.

IV. Results and Discussion

The characterization and comparative results of cylindrical Li-ion batteries are analyzed under different operating conditions to evaluate the battery performance and also results were validated with literature data [50-55]. The simulated characteristics of a cylindrical rechargeable battery and results are discussed below.

A. Electrochemical Characteristics

The electrochemical results help to evaluate the physical and electrochemical properties of the rechargeable battery. Therefore, a cyclic voltammetry (CV) curve has been plotted which helps to determine the electrochemical reactivity and transport properties of a lithium-ion battery [32-34]. In this CV test, the potential varies linearly as a function of time is applied to the working electrodes [33].

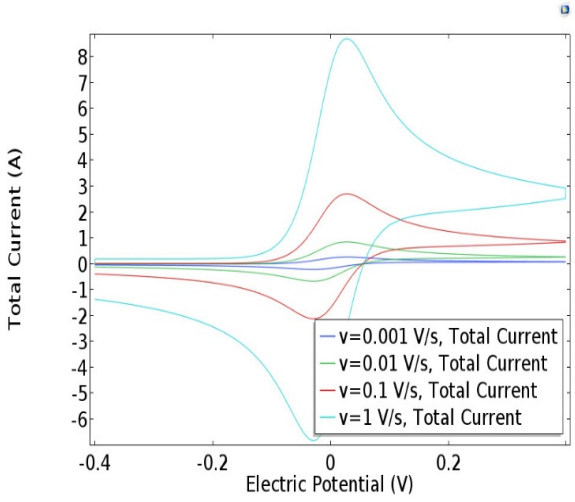

Figure 2. Cyclic-voltammetry curve

Fig. 2 shows the recorded cyclic voltammetry curve which determines the relation between the transport chemical species. It also represents the diffusion of lithium ions in the battery and the electrode kinetics [33].

The results are plotted at the variable potential range, in which parametric sweep was used to record the graph at different scan-rates The CV result suggests that at a lower scan rate of 0.001 V/s, the potential is very low due to that the oxidation reaction is not taken place and hence the current is negligible. It also shows that once the potential starts increasing the oxidation reaction becomes accelerated and the current also starts increasing. Once the oxidation reaction has consumed reactant at the electrode surface then the current becomes limited by the rate of transport at the working electrode. Therefore, the highest peak current of 8Ah has been observed at a higher scan rate of 1 v/s after the peak of Volta metric current. It starts falling independent of the potential rate. This region of the CV curve denotes the diffusion-controlled or transport-controlled region. Similarly, the other characteristics are simulated and analyzed to determine the charge and discharge characteristics of the LMO battery.

B. Rate Capability Characteristics

The comparative results of two different types of anodes (graphite and MCMB) were plotted on the cylindrical Li-ion battery in which, two combinations of different anode material have been investigated. The two-electrode pair was formulated, one was LMO/Graphite and the other one was LMO/Carbon (MCMB). The only difference between both these electrode pairs was the change of anode material, through which cathode material was investigated and evaluated during its characterization.

In this 2D model, the theoretical results are briefly explained and simulated with the help of Multiphysics software but all these results are theoretically simulated and to validate these results the experimental data was explained from the literature [56-60].

A 2D model of a Lithium-ion battery was simulated to understand the behavior of $LiMn_2O_4$ cathode material and the rate capability of the battery was investigated [34-36].

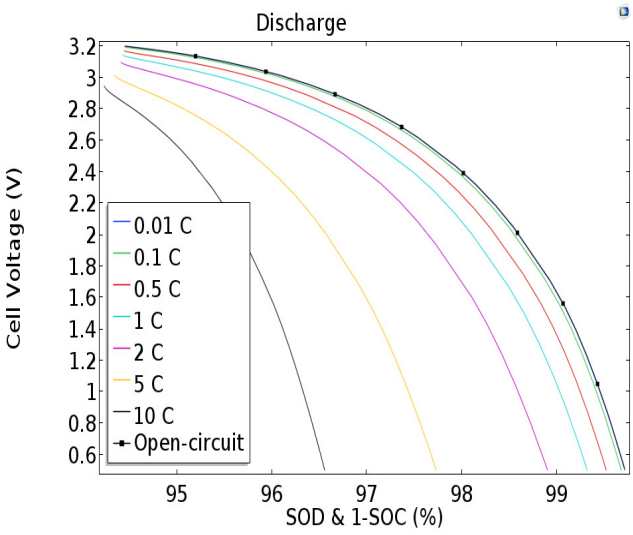

Figure 3. Discharge characteristics of LMO/Graphite

Initially, the battery was discharged from its charge state and then fully charged from its discharged state at different C-rates and the discharge characteristics are plotted as shown in the Fig. 3.

In Fig. 3, the LMO/graphite discharge curve represents the discharge capacity of the battery in an open circuit which comes to be 99.5% of its battery capacity.

As the load current starts increasing the voltage drop (polarization) across the battery is also observed to be increasing and it results in a decrement in the capacity of the

battery. Hence, when the load current was increased up to 10 C rate, the capacity is reached approximately 96.7% of the ideal battery capacity.

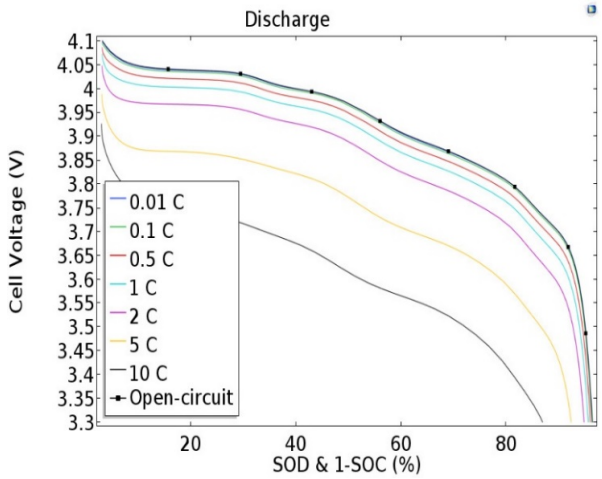

Figure 4. Discharge characteristics of LMO/carbon (MCMB)

In Fig. 4, the LMO/carbon (MCMB) discharge curve represents the same phenomenon but its capacity is found lesser as compared to LMO/graphite electrode and at 10 C rate, the battery capacity is decreased up to 88% of its full capacity. This shows that the LMO/graphite electrode material has better rate capability at a high C-rate than that of the LMO/carbon (MCMB) electrode.

Similarly, the experimental data were reported by various researchers, in which $LiMn_2O_4$/graphite electrodes has 117 mAh/g discharge capacity. This capacity was retended 94.6% at 10 C rate till the battery was operated at 100 cycles [56-58].

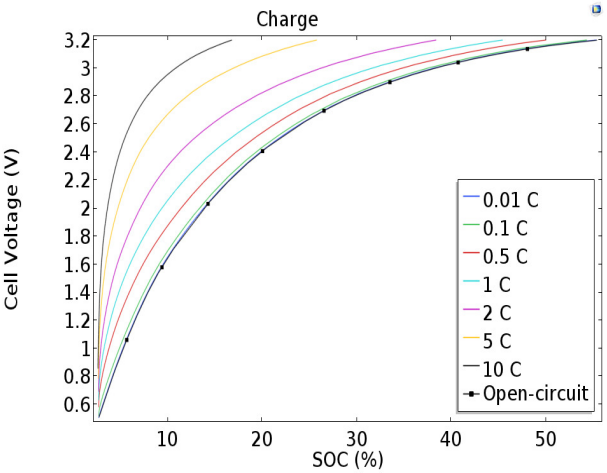

Figure 5. Charge characteristics of LMO/Graphite

However, for $LiMn_2O_4$/Carbon electrodes has 114mAh/g discharge capacity and this capacity was retended 90% of its full capacity after certain cycles at 10C rate [59-60]. Hence, this experimental data has validated the theoretical results in which LMO/graphite has better capacity then LMO/Carbon. The charge characteristics of the cylindrical Li-ion battery have also been investigated and it is found that the charge capacity of the battery was lower than the discharge capacity. The reason for this phenomenon is that the medium-high current load of the active electrode material and cell voltage of the battery lies within the stability window of the electrolyte [36-40].

The charge characteristics of LMO/graphite have been plotted in the Fig. 5 and it is found that even though the charge capacity was lesser than the discharge capacity, polarization is observed in the discharge curve having the same plateau at 3.2 V. It clearly indicates that the $LiMn_2O_4$/graphite was stable in nature during oxidation and reduction process.

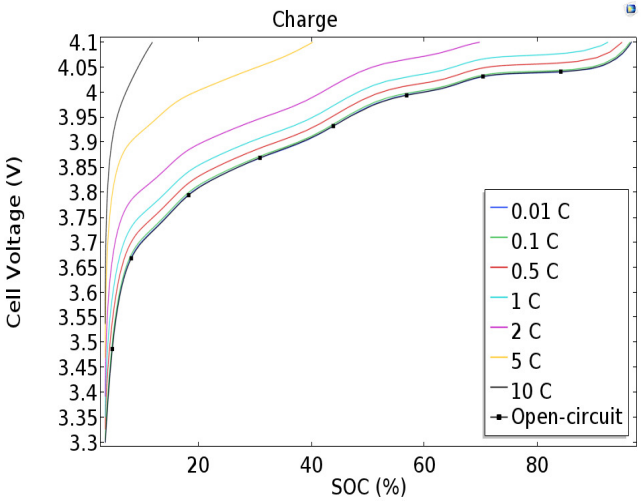

Figure 6. Charge characteristics of LMO/Carbon (MCMB)

Fig. 6 shows the charge characteristics of the LMO/MCMB where it is observed that its charge capacity is also lower than the discharge capacity but as compared to the LMO/graphite, it has a lesser charge capacity during 10 C-rate. Therefore, it indicates that LMO/graphite has better battery performance than the LMO/carbon (MCMB).

C. Ragone Characteristics

The ragone plot is obtained to find out the energy and power output in both the combination of batteries i.e., LMO/Graphite and LMO/Carbon (MCMB). The ragone plot helps to calculate the energy output using global ordinary differential equation (ODEs) and Differential algebraic equation (DAEs) interface according to equation 10.

$$W = \int_0^T (I.E_{cell})dt \tag{10}$$

where I represent the current in the battery and E_{cell} represent the cell voltage of the battery [45].

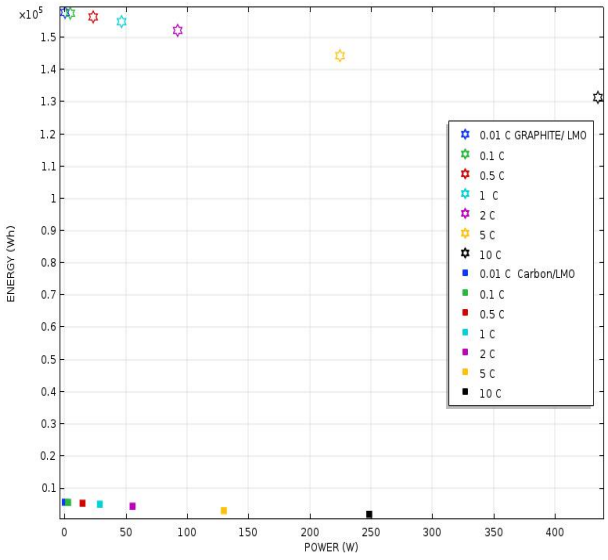

Figure 7. Ragone plot

In Fig. 7, the power output was plotted by dividing the energy by the total discharge time and the event interface has been used to restrict the operation of the battery within the upper and lower cut-off voltages [46-51].

The ragone curve in the Fig. 7, shows that LMO/carbon (MCMB)has lower energy as compared to LMO/Graphite which is due to the lower cell voltage of the battery. Hence, good rate capability may be achieved using the LMO/Graphite electrode material.

V. Conclusion

In this paper, a 2D electrochemical model of lithium-ion battery has been developed on COMSOL Multiphysics software. The formulation of the electrochemical model has been done with the help of various input parameters and the developed mathematical model is validated against the literature data. Simulation has been performed for the developed model to find out the battery performance in terms of cyclic voltammetry, rate capability i.e., energy and power within the defined limits. The simulation results confirm that the battery performance has improved by changing the design variables and chemistry of the battery. The cyclic voltammetry shows good electrochemical reactivity and transport properties in the designed Li-ion battery. Further, the comparison of two different types of electrode pairs, namely LMO/Graphite and LMO/MCMB has been conducted, where LMO/Graphite has shown approximately 96% discharge capacity of its full state of charge at 10C rate as compared to the 88% in the case of LMO/MCMB. Also, the LMO/graphite has shown better energy capacity as compared to the LMO/MCMB making it a suitable material for Li-ion battery.

Acknowledgment

The authors are thankful to LIBT Lab, Department of Applied Physics, Delhi Technological University, New Delhi for providing support to carry out this research work.

References

[1] M. Hannan, M. Hoque, A. Mohamed, A. Ayob, "Review of Energy Storage Systems for Electric Vehicle Applications: Issues and Challenges" Renewable and Sustainable Energy Reviews 69, p.p. 771-789, 2017. doi:10.1016/j.rser.2016.11.171

[2] X. Lu, "Application of the Nernst-Einstein Equation to Concrete" Cement, and Concrete Research 27 (2), p.p. 293-302,1997 doi:10.1016/S0008-8846(96)00200-1

[3] M. Park, X. Zhang, M.chung, G. B. Less, A. M. Sastry, A Review of Conduction Phenomenon in Li-ion batteries" Journal of Power Sources 195 (24), 7904-7929, 2010. doi:10.1016/2010.06.060

[4] T. R. Tanim, C. D. Rahn, C. Y .Wang, A Temperature Dependent, Single particle, Lithium ion Cell Model including Electrolyte Diffusion" Journal of Dynamic Systems, Measurement, and Control, vol.1, p.p. 137, 2015. doi:10.1016/j.jpowsour.2010.06.060

[5] R. Darling, J. Newman, "Modeling a Porous Intercalation Electrode with Two Characterstic Particle Sizes" Journal of the Electrochemical Society, vol. 144 (12), p.p. 4201-4208, 1997. doi:10.1149/1.1848073

[6] J. Xu, Y. Wu, S. Yin, "Investigation of Effects of Design Parameters on the Internal Short-circuit in cylindrical lithium-ion batteries" RSC advances 7 (24), 14360-14371 (2017). doi:10.1039/C6RA27892B

[7] A. Nazari, S. Farhad, "Heat Generation in Lithium ion Batteries with Different Nominal Capacities and Chemistries" Applied Thermal Engineering 125, p.p. 1501-1517, 2017. doi:10.1016/j.applthermaleng.2017.07.126

[8] J. Baron, G. Szymanski, J. Lipkowski, "Electrochemical Methods to Measure Gold Leaching Current in an Alkaline Thiosulfate Solution" Journal of Electroanalytical Chemistry 662 (1), p.p. 57-63, 2011. doi:10.1016/j.jelechem.2011.03.001

[9] S. Venkatraman, J. Choi, A. Manthiram, "Factors Influencing the Chemical Lithium Extraction Rate from Layered LiNi1-y-zCoyMnzO2 cathodes" Electrochemistry Communications 6 (8), p.p. 832-837, 2004. doi:10.1016/j.elecom.2004.06.004

[10] M. Wu, B. Xu, and C. Ouyang, "Physics of Electron and Lithium ion Transport in Electrode Materials of Li-ion Batteries" Chinese Physics B 25 (1), 018206 2015. doi:10.1088/1674-1056/25/1/018206

[11] E. Hosseinzadeh, J. Marco, P. Jennings, "Electrochemical- Thermal Modelling and Optimization of Lithium-ion Battery Design Parameters Using Analysis of Variance" Energies 10 (9), 1278 2017. doi:10.3390/en10091278

[12] A. Jokar, B. Rajabloo, M. Desilets, M. Lacroix, "Reviews of Simplified Pseudo-Two-Dimensional Models of Lithium-ion Batteries"Journal of Power Sources 327, p.p. 44-55, 2016. doi:10.1016/j.jpowsour.2016.07.036

[13] N. Jin, D. L. Danilov, P. M. Van den Hof, M. Donkers, "Optimization of Current Excitation for Identification of Battery Electrochemical Parameters based on Analytic Sensitivity Expression" International Journal of Energy Research 42 (7), p.p. 2417-2430, 2018.doi:10.1002/er.4022

[14] K. Uddin, S. Perera, W. D. Widanage, L. Somerville, J. Marco, Characterising Lithium-ion Battery Degradation through the dentification and Tracking of Electrochemical Battery Model Parameters" Batteries 2 (2), 13, 2016. doi:10.3390/batteries2020013

[15] Y. Huang, H. Lai, "Effect of Discharge Rate on Electrochemical and Thermal Characterstics of LiFePO4/Graphite Battery" Applied Thermal Engineering 157, 113744 2019. doi:10.1016/j.applthermaleng.2019.113744

[16] J. Yang, X. Wei, H. Dai, J. Zhu, X. Xu, "Lithium-ion Battery Internal Resistance Model Based on the Porous Electrode Theory" IEEE Vehicle Power and Propulsion Conference (VPPC), 2014. doi:10.1109/VPPC.2014.7007096

[17] P. Wu, J. Romberg, H. Ge, Y. Zhang, J. Zhang, Electrochemical-Thermal Coupled Model of Lithium-Ion Batteries for Low Temperature Charging, in: Soc. Automot. Eng. SAE-China Congr., Springer, 2016: pp. 123-132. doi:10.1007/978-981-10-3527-2_12

[18] J. Newman, W. Tiedmann, "Porous-Electrode Theory with Battery Applications" AICHE Journal, vol. 21(1), p.p. 25-41, 1975. doi:10.1002/aic.690210103

[19] S. Srivastav, P. Tammela, D. Brandell, M. Sjodin, "Understanding Ionic Transport in Polyyyrole/Nanocellulose Composite Energy Storage Devices" Electrochimica Acta 182, p.p. 1145-1152, 2015. doi:10.1016/j.electacta.2015.09.084

[20] A. Melcher, C. Ziebert, M. Rohde, H. J. Seifert, "Modelling and Simulation of Thermal Runaway Behavior of Cyclindrical Li-ion Cells Computing of Critical Parameters" Energies 9 (4), 292, 2016. doi:10.3390/en9040292

[21] C. Ziebert, A. Melcher, B. Lei, W. Zhao, M. Rohde, H. Seifert, "Electrochemical-Thermal Characterization and Thermal Modeling for Batteries" Emerging Nanotechnologies in Rechargeable Energy Storage Systems (Elsevier), pp. 195-229, 2017. doi:10.1016/ 0-323-42977-1.00006-6

[22] K. Li, J. Yan, H. Chen, Q. Wang, "Water Cooling Based Strategy for Lithium-ion Battery Pack Dynamic Cycling for Thermal Management System" Applied Thermal Engineering 132, p.p. 575-585, 2018. doi:10.1016/j.applthermaleng.2017.12.131

[23] Z. Khalik, H. J. Bergveld, M. Donkers," Aging-Aware Charging of Lithium-ion Batteries using an Electrochemistry-Based Model with Capacity-loss Side Reactions" American Control Conference (ACC), 2020. doi:10.23919/ACC45564.2020.9147404

[24] J. Li, D. Wang, L. Deng, Z. Cui, C. Lyu, L. Wang, M. Pecht, "Aging Mode Analysis and Physical Parameter Identification based on a Simplified Electrochemical Model for Lithium-ion Batteries" Journal of Energy Storage 31, 101538, 2020. doi:10.1016/j.est.2020.101538

[25] Y. Qi, T. Jang, V. Ramadesigan, D. T. Schwartz, V. R. Subramanian, "Is There a Benefit in Employing Graded Electrodes for Lithium-ion Batteries?" Journal of The Electrochemical Society 164 (13), A3196 2017. doi:10.1149/2.1051713jes

[26] N. Li, L. Fu, K. Jiang, "Gas Evolution and The Effects on Ionic Transport inside the Lithium-ion Battery" Engineering Computations, 2019.

[27] P. R. Nileshwar, A. McGordon, T. Ashwin, D. Greenwood, "Parametric Optimization Study of a Lithium-ion Cell" Energy Procedia 138, p.p. 829-83, 2017. doi:10.1016/j.egypro.2017.10.088

[28] J. Xu, B. Liu, X. Wang, D. Hu, "Computational model of 18650 Lithium-ion Battery with Coupled Strain Rate and SOC Dependencies "Applied Energy 172, p.p. 180-189 2016. doi:10.1016/j.apenergy.2016.03.108

[29] Y. Liu, S. Tang, L. Li, F. Liu, L. Jiang, M. Jia, Y. Ai, C. Yao, H. Gu, "Confining Ultrasmall Bimetallic Alloys in Porous N-Carbon for Use

as Scalable and Sustainable Electrocatalysts for Rechargeable Zn-air Batteries" Journal of Alloys and Compounds, 156003, 2020.

[30] Y. Dai, V. Srinivasan, "On Graded Electrode Porosity as a Design Tool for Improving the Energy Density of Batteries" Journal of The Electrochemical Society 163 (3), A406, 2015. doi:10.1149/2.0301603jes

[31] S. Panchal, I. Dincer, M. Agelin-Chaab, R. Fraser, M. Fowler, "Transient Electrochemical Heat Transfer Modeling and Experimental Validation of a Large Sized LiFePO4/Graphite Battery" International Journal of Heat and Mass Transfer 109, p.p. 1239-1251, 2017. doi:10.1016/j.ijheatmasstransfer.2017.03.005

[32] K. Somasundaram, E. Birgersson, A. S. Mujumdar, "Thermal-Electrochemical Model for Passive Thermal Management of a Spiral-Wound Lithium-ion Battery" Journal of Power Sources 203, p.p. 84-96, 2012. doi:10.1016/j.jpowsour.2011.11.075

[33] S. Wang, J. Wang, Y. Gao, "Exfoliation of Covalent Organic Frameworks into Few-Layer Redox-Active Nanosheets as Cathode Materials for Lithium-ion Batteries (2017),139, 12, 4258-4261. doi:10.1021/jacs.7b02648

[34] K. Shaju, G. S. Rao, B. Chowdari, "X-Ray Photoelectron Spectroscopy and Electrochemical Behaviour of 4V Cathode, Li (Ni1/2Mn1/2) O2 Electrochimica Acta 48 (18), p.p. 2691-2703, 2003. doi:10.1016/S0013-4686(03)00088-4

[35] H. Li, C. Liu, A. Saini, Y. Wang, H. Jiang, T. Yang, L. Chen, C. Pan, H. Shen, "Coupling Multi-Physics Simulation and Response Surface Methodology for the Thermal Optimization of Ternary Prismatic Lithium-ion Battery" Journal of Power Sources 438, 226974, 2019. doi:10.1016/j.jpowsour.2019.226974

[36] C. Edouard, M.Petit, C. Forgez, J.Bernard, R.Revel, "Parameter Sensitivity Analysis of a Simplified Electrochemical and Thermal Model for Li-ion Batteries Aging" Journal of Power Sources, vol. 33, p.p. 482-494, 2016. doi:10.1016/j.jpowsour.2016.06.030

[37] L. Zhang, C. Lyu, L. Wang, W.Luo, K. Ma, "Thermal-Electrochemical Modeling and Parameter Sensitivity Analysis of Lithium-ion Battery" Chemical Engineering, Vol. 33, p.p. 943-948, 2013.

[38] Y. H. Chen, C. W. Wang, X. Zhang, A. M. Sastry, "Porous Cathode Optimization for Lithium Cells: Ionic and Electronic Conductivity, Capacity, and Selection of Materials" Journal of Power Sources, vol. 195(9), p.p. 2851-2862, 2010. doi:10.1016/j.jpowsour.2009.11.044

[39] W. Wu, X. Xiao, X. Huang, "The Effect of Battery Design Parameters on Heat Generation and Utilization in a Li-ion cell" Electrochemica Acta, vol. 83, p.p. 227-240, 2012. doi:10.1016/j.electacta.2012.07.081

[40] S. Golmon, K. Maute, M. L. Dunn, "A Design Optimization Methodology for Li+ Batteries" Journal of Power Sources, vol.253, p.p. 239-250, 2014. doi:10.1016/j.jpowsour.2013.12.025

[41] J. Li, Y. Cheng, L. Ai, M. Jia, S. Du, B. Yin, S. Woo, H. Zhang, "3D Simulation on the Internal Distributed Properties of Lithium-ion Battery with Planar Tabbed Configuration" Journal of Power Sources, vol. 293, p.p. 993-1005, 2015. doi:10.1016/j.jpowsour.2015.06.034

[42] J. Li, Y. Cheng, M. Jia, Y. Tang, Y. Lin, Z. Zhang, Y. Liu, "An Electrochemical-Thermal Model Based on Dynamic Responses for Lithium Iron Phosphate Battery" Journal of Power Sources, vol. 255, p.p. 130-143, 2014. doi:10.1016/j.jpowsour.2014.01.007

[43] A. M. Bizeray, S. Zhao, S. R. Duncan, D. A. Howey, "Lithium-ion Battery Thermal-Electrochemical Model-Based State Estimation using Orthogonal Collocation and a Modified Extended Kalman Filter" Journal of Power Sources, vol. 296, p.p. 400-412, 2015. doi:10.1016/j.jpowsour.2015.07.019

[44] J. M. Tarascon, M. Armand, "Issues and Challenges Facing Rechargeable Lithium Batteries" Materials for Sustainable Energy: A Collection of Peer-Reviewed Research and Review Articles from Nature, p.p. 171-179, 2011. doi:10.1142/9789814317665_0024

[45] W. Tong, K. Somasundaram, E. Birgersson, A. S. Mujumdar, C. Yap, "Thermal-Electrochemical Model for Forced Convection Air Cooling of a Lithium-ion Battery Module" Applied Thermal Engineering 99, 672-682 (2016). doi:10.1016/j.applthermaleng.2016.01.050

[46] M. Doyle, T.F. Fuller, J. Newman, "Modelling of Galvanostatic Charge and Discharge of the Lithium/Polymer insertion Cell" Journal of the Electrochemical Society, vol. 140(6), p.p. 1526, 1993. doi:10.1149/1.2221597

[47] M. Doyle, J. Newman, A. S. Gozdz, C. N. Schmutz, J.M. Tarascon, "Comparison of Modeling Predictions with Experimental Data from Plastic Lithium-ion Cells" Journal of Electrochemical Society, vol. 143(6), 1890, 1996. doi:10.1149/1.1836921

[48] T. F. Fuller, M. Doyle, J. Newman, "Simulation and Optimization of the Dual Lithium-ion Insertion Cell" Journal of Electrochemical Society, vol. 141(1), 1, 1994. doi:10.1149/1.2054684

[49] L. L. Lam, R. B. Darling, "Theory of Battery Aging in a Lithium-ion Battery: Capacity Fade, Non-Linear Ageing and Lifetime Prediction" Journal of Power Sources, vol. 276, p.p. 195-202, 2015.

[50] P. Arora, R. E. White, M. Doyle, "Capacity Fade Mechanism and Side Reactions in Lithium-ion Batteries" Journal of Electrochemical Society vol. 145 (10), 3647, 1988. doi:10.1149/1.1838857

[51] P. Ramadass, B. Haran, R. White, B. N. Popov, "Mathematical Modeling of the Capacity Fade of Li-ion Cells" Journal of Power Sources, vol. 123 (2), p.p. 230-240, 2003. doi:10. 1016.S0378.7753(03)00531-7

[52] F. Laman and K. Brandt, "Effect of Discharge Current on Cycle Life of a Rechargeable Lithium Battery" Journal of Power Sources, vol. 24 (3), p.p. 195-206, 1988. doi:10.1016/0378-7753(88)80115-0

[53] A. Dogan, S. Bahceci, F. Daldaban, M. Alci, "Optimization of Charge/Discharge Co-ordination to Satisfy Network Requirements Using Heuristic Algorithms in Vehicle-to-Grid Concept" Advances in Electrical and Computer Engineering, vol. 18 (1), p.p. 121-131, 2018. doi:10.4316/AECE.2018.01015

[54] S. Zhang, X. Guo, X. Zhang, "Modelling of Back-Propogation Neural Network Based State-of-Charge Estimation for Lithium-ion Batteries with Consideration of Capacity Attenuation" Advances in Electrical and Computer Engineering, vol. 19 (3), p.p. 3-11, 2019. doi:10.4316/AECE.2019.03001

[55] D. Petreus, D.Moga, R. Galatus, R. A. Munteanu, "Energy Harvesting with Supercapacitor-Based Energy Storage" Advances in Electrical and Computer Engineering, vol. 8 (2), p.p. 15-22, 2008. doi:10.4316/aece.2008.02003

[56] Y. J. Liu, X. H. Li, H. J. Giu, "Overcharge performance of LiMn2O4 / graphite battery with large capacity" J. Cent. South Univ. Technol. Vol. 16, p.p. 0763-0767, 2009. doi:10.1007/s11771-009-0127-y

[57] W. A. Appiah, J. Park, S. Byun, M. H. Ryou, Y. M. Lee, "A Mathematical model for cyclic aging of spinel LiMn2O4 /Graphite Lithium-ion cells" Journal of the Electrochemical Society, vol. 163 (13), p.p. A2757-A2767, 2016. doi:10.1149/2.1061613jes

[58] A. J. Smith, J.C. Burns, J. R. Dahn, "High-precision differential capacity analysis of LiMn2O4/Graphite cells" Electrochemical and solid-state letters, vol. 14 (4), p.p. A39, 2011. doi:10.1149/1.3543569

[59] J. Caihua, T. Zilong, D. Shiqing, H. Ye, W. Shitong, Z. Zhong Tai, "High performance Carbon-Coated mesoporous LiMn2O4 cathode materials synthesized form a novel hydrated layered -spinel lithium manganate composite" Journal of RCS Advances, vol. 7, p.p. 3746-3751, 2017. doi:10.1039/C6RA25802F

[60] S. Vadivel, P. Nutthaphon, W. Juthaporn, S, Montree, "High-performance spinel LiMn2O4@carbon core-shell cathode materials for Li-ion Batteries" Journal of Sustainable Energy & Fuels, vol. 3, p.p. 1988-1994, 2019. doi:10/1039/C9SE00274J

[61] S. Sharma, A. K. Panwar, M. M. Tripathi, Storage technologies for electric vehicles, J. Traffic Transp. Eng. Engl. Ed. 7 (2020) 340-361. doi:10.1016/j.jtte.2020.04.004